Electrical control of Dzyaloshinskii-Moriya interactions in magnetic Weyl semimetals

Yuriy G. Semenov,[1,2] Xinyi Xu,[1] James A. Boulton,[1] and Ki Wook Kim[1,3,*]

[1]*Department of Electrical and Computer Engineering, North Carolina State University, Raleigh, North Carolina 27695, USA*

[2]*V. Lashkaryov Institute of Semiconductor Physics, National Academy of Sciences of Ukraine, Kyiv 03680, Ukraine*

[3]*Department of Physics, North Carolina State University, Raleigh, North Carolina 27695, USA*

(Received 11 July 2023; accepted 6 October 2023; published 19 October 2023)

The Dzyaloshinskii-Moriya interaction (DMI) is known to be responsible for multiple phenomena in magnetic materials. In the conventional description as a perturbation of the superexchange interaction by the spin-orbit coupling, the strength of the DMI is only weakly sensitive to the external fields, making its control difficult in spintronic applications. In this work, we show that an electrical modulation of the DMI may actually be possible in magnetic Weyl semimetals (WSMs). Specifically, it is theoretically illustrated that an antisymmetric indirect spin-spin interaction identified recently as an alternative mechanism for the DMI can result in the desired sensitivity to the external electric and magnetic fields via a redistribution of Weyl fermions among nodes of opposite chirality. This chiral anomaly enabled approach becomes particularly prominent in WSMs with inversion symmetry, in which the conventional DMI is not allowed. Numerical estimations suggest that moderate electric and magnetic fields of $\sim 10^3$–10^4 V/cm and ~ 1 T can induce a sufficiently strong change in the DMI. The impact of this externally modulated DMI on the manipulation of magnetic textures, including skyrmions in WSMs, is also discussed.

DOI: 10.1103/PhysRevB.108.134428

I. INTRODUCTION

Over the past few decades, a range of exotic phenomena originating from the spin-orbit interaction was found and led to a second wind in relativistic physics in solids. An antisymmetric superexchange interaction in the form of Dzyaloshinskii-Moriya interaction (DMI) is one such example of the nontrivial manifestation of this interaction [1,2]. It explains the appearance of a weak magnetization caused by a tilt in the sublattice magnetizations of antiferromagnets without the intervention of an external magnetic field. The more prominent effects of the DMI, on the other hand, are related to the formation of inhomogeneous magnetic structures such as helical magnetic textures and spin glass [3,4]. Of particular interest among them are localized structures (e.g., domain walls, solitons, and skyrmions), in which the strength of the DMI tends to exceed some critical values [5,6]. Accordingly, the problem of how to control and manipulate the DMI has become especially critical for emerging spintronic device applications. While strain can be used to induce and control the DMI [7,8], it is generally more desirable if this control can be achieved through the application of fields (particularly, the electric field) without causing structural changes. However, the influence of an external electric field is generally much smaller than the intra-atomic counterparts in the conventional description of the DMI as a perturbation of the superexchange interaction by spin-orbit coupling. This general statement remains the case even in instances showing a comparatively more robust dependence such as modulation via the field-induced structural distortion in a two-dimensional ferromagnet [9], structural inversion asymmetry at the interface [10,11], and defect migration [12], as well as modulation via an electric current [13,14]. Accordingly, it may be necessary to look for an alternative mechanism of asymmetrical spin-spin coupling and a material system that can provide the desired sensitivity to the fields.

One promising possibility is Weyl semimetals (WSMs), in which the indirect spin-spin interaction via Weyl fermions supports the skew-symmetric spin-spin interaction (thus, a potential origin of the DMI) along with the conventional Ruderman-Kittel-Kasuya-Yosida (RKKY) isotropic exchange interaction [15–18]. Normally, the interference of indirect spin-spin interactions caused by the reciprocal electron scattering between nodes of opposite chirality does not survive (i.e., full cancellation). Similarly, the intranode spin-dependent fermion relaxation in the WSM cannot induce the net DMI through the compensation by Weyl nodes of opposite chirality. An interesting point to note is that this symmetry can be readily broken in WSMs by the external electric and magnetic fields (i.e., **E** and **B**, respectively) as long as these fields are not normal to each other. In the present study, we show that the resulting imbalance in the Weyl node population (i.e., a direct manifestation of the chiral anomaly) can become a mediator of the DMI between the remote spin pairs in WSMs. More precisely, the strength of the induced DMI is found to be proportional to a vector relation $\mathbf{d}_D(\mathbf{E}\cdot\mathbf{B})$, where the WSM material parameters determine the constant vector $\mathbf{d}_D$. Subsequent calculations show that a moderate electric field of around 10^3–10^4 V/cm along with a magnetic field of ~ 1 T can produce a DMI sufficiently strong to modulate local magnetic textures such as magnetic skyrmions. This

*kwk@ncsu.edu

remote RKKY-mediated mechanism is expected to provide the dominant contribution to the DMI in magnetic WSMs with centrosymmetry.

II. THEORETICAL MODEL

A. Basic formulation

As a comprehensive analysis of the RKKY interaction in the WSMs is already available in the literature [18], we can start by applying this approach to a ferromagnetic (FM) WSM with a pair of Weyl nodes (chirality $\chi = \pm 1$) separated in momentum space. In contrast to the case of conventional massive electronic dispersion, the sum over the virtual Weyl fermions diverges as long as the massless linear dispersion law persists with a constant Fermi velocity v_F. This "ultraviolet" divergence is naturally resolved in actual crystals, in which the electronic structure mimics the WSM only in the vicinity of momentum space around the Weyl points. As the contribution to the indirect spin-spin interaction is thought to be small outside the linear region, a cutoff in energy $\mathcal{E}_c$ and, correspondingly, in momentum Λ $(= \mathcal{E}_c/\hbar v_F)$ can be introduced to limit the consideration to only the relevant range near each Weyl node. This approximation based on the sharp cutoff Λ in momentum or energy is considered adequate when describing the spin-spin interaction in intrinsic WSM magnets, in which local moments are rather densely populated (thus, on a relatively short length scale) [18]. An alternative treatment based on a full tight-binding band like what was done for magnetic impurities in graphene [19] could make the calculation more accurate but is outside the scope of the current work.

The RKKY-type model provides an adequate description of the asymmetrical interaction for the spin pair $\mathbf{S}_j$ and $\mathbf{S}_{j'}$ located at lattice sites $\mathbf{r}_j$ and $\mathbf{r}_{j'}$ in the following form:

$$H_{j,j'} = \mathbf{D}_{j,j'} \cdot (\mathbf{S}_j \times \mathbf{S}_{j'}), \tag{1}$$

where the vector contribution of each Weyl node χ can be written as [18]

$$\mathbf{D}^{(\chi)}_{j,j'} = \chi \frac{2(a\Lambda)^6 J^2}{(4\pi)^4 \mathcal{E}_c} f\left(\frac{2\mu}{\mathcal{E}_c}, \Lambda r_{j,j'}\right) \widehat{\mathbf{r}}_{j,j'}. \tag{2}$$

Here, a, J, and μ denote the lattice constant, carrier-ion exchange interaction, and chemical potential, respectively; $r_{j,j'} = |\mathbf{r}_j - \mathbf{r}_{j'}|$, and $\widehat{\mathbf{r}}_{j,j'}$ is a unit vector directed along $\mathbf{r}_j - \mathbf{r}_{j'}$. The full expression for $f(x, y)$ is rather complicated but can be well approximated by an analytical function for $x \lesssim 1$:

$$f(x, y) \approx x^3 \varphi(y), \tag{3}$$

where

$$\varphi(y) = -\pi \frac{\sin[0.04y + y^3/(40 + y^2)]}{1 + 0.22y^3}. \tag{4}$$

The oscillatory behavior predicted in the indirect DMI [Eq. (4)] differs substantially from that associated with the RKKY interaction in the conventional crystals. For one, the oscillations start with $f(x, y) \to 0$ at $y \sim r_{j,j'} \to 0$ and then become aperiodic, reaching the maximum at $y \equiv \Lambda r_{j,j'} \sim 2.5$. By contrast, the maximum of the indirect RKKY interaction in conventional magnets corresponds to the shortest interion distance. In addition, the chemical potential μ in Eq. (2) controls the amplitude of $D_{j,j'}$ but not the period of oscillations, whereas both are affected in the latter. Note that the simple analytical approximation given in Eq. (4) represents the best fit to the actual dependence of $\varphi(y)$ in the range $y \lesssim 15$ relevant to the numerical calculation (consistent with the truncation discussed in Sec. III B). For larger y (e.g., $r_{j,j'} \to \infty$), $\varphi(y)$ reveals a slower decay of y^{-2} [18], which may be important in other applications of the remote DMI.

As expected, Eqs. (2) and (3) clearly illustrate the absence of the DMI in a centrosymmetric WSM with an equal chemical potential for the Weyl cones. Namely, the + and − signs of chirality χ would cancel exactly the contributions from each node for the given Weyl pair. However, this is not the case if the external fields support an imbalance in the node populations. As is well known, such a possibility can be realized in a WSM with broken time reversal symmetry via the application of nonorthogonal electric and magnetic fields. These fields induce a chiral current of spin-polarized Weyl fermions carrying a charge q_e between the Weyl cones of $\chi = \pm 1$ and can establish an imbalance in the chemical potential between two nodes with opposite chirality (i.e., μ_+ vs μ_-). While the internode fermion scattering may diminish the net spin polarization, it is unlikely to cancel out the effect (i.e., the chiral anomaly) completely. The resulting axial chemical potential $\mu_5 = (\mu_+ - \mu_-)/2$ becomes proportional to the strengths of both fields.

In the case of a weak magnetic field (e.g., $\hbar v_F q_e B \ll \mu_5^2$) and a non-negligible temperature T_0 (in units of energy), the effect of a thermal population in the Landau levels needs to be accounted for as [20,21]

$$\mu_5 = \frac{3\hbar v_F^3 q_e^2 \tau}{2(\pi T_0)^2 + 6\mu_0^2} \frac{\mathbf{E} \cdot \mathbf{B}}{c}, \tag{5}$$

where $\mu_0 = (\mu_+ + \mu_-)/2$, c is the speed of light, and τ is the characteristic relaxation time of the internode scattering. Then, the net nonzero contribution of both nodes to the DMI, provided $\mu_5 \ll \mu_0$, becomes

$$\mathbf{D}_{j,j'} = \widehat{\mathbf{r}}_{j,j'} \frac{2(a\Lambda)^6 J^2}{(4\pi)^4 \mathcal{E}_c} \frac{6\mu_0^2 \mu_5}{\mathcal{E}_c^3} \varphi(\Lambda r_{j,j'}). \tag{6}$$

Combining this expression with Eq. (5) defines the vector

$$\mathbf{D}_{j,j'} = \widehat{\mathbf{r}}_{j,j'} \, \varphi(\Lambda r_{j,j'}) \Delta_{\mathrm{DM}}, \tag{7}$$

where

$$\Delta_{\mathrm{DM}} = \frac{18(a\Lambda)^6 J^2 \mu_0^2}{(4\pi)^4 \mathcal{E}_c^4} \frac{\hbar v_F^3 q_e^2 \tau}{(\pi T_0)^2 + 3\mu_0^2} \frac{\mathbf{E} \cdot \mathbf{B}}{c}. \tag{8}$$

As can be seen, an increase in the chemical potential can enhance the DMI when $\mu_0 < T_0$, beyond which point the dependence weakens and saturates as $\mu_0 \gg T_0$. More importantly, the sign of Δ_{DM} shows an explicit dependence on the polarity of the applied field. This property selects the favorable twisting direction of the DMI effect (i.e., clockwise or counterclockwise), which is described in greater detail in Sec. III. The notation adopted above supposes the Gaussian system of units; the SI system would impose $c = 1$ instead.

B. Application to micromagnetic simulations

The effect of the long-range RKKY-mediated DMI on the formation of inhomogeneous magnetic texture can be

efficiently studied via micromagnetic simulations. Since the properties in each discretized cell (located at $\mathbf{n}$) are assumed to be homogeneous in the numerical modeling while the actual DMI is between two discrete atoms (i.e., located at lattice sites $\mathbf{r}_j$ and $\mathbf{r}_{j'}$), an approach that effectively averages these interactions is necessary. To that end, let us consider a spin $\mathbf{S}_j$ in a cell $\mathbf{n}$ (i.e., $j \in \mathbf{n}$). With the contributions from all other $\mathbf{S}_{j'}$ (for which $\langle \mathbf{S}_{j'} \rangle$ denotes the mean value), the DMI-mediated energy of this spin $\mathbf{S}_j$ can be expressed as

$$\mathcal{E}_j = g\mu_B \mathbf{B}_j \cdot \langle \mathbf{S}_j \rangle = \left(\sum_{j'} [\langle \mathbf{S}_{j'} \rangle \times \mathbf{D}_{j,j'}] \right) \cdot \langle \mathbf{S}_j \rangle. \quad (9)$$

If the size of the magnetic texture sufficiently exceeds the cell dimension d (with volume V_s), a slowly varying magnetization $\mathbf{M}(\mathbf{r})$ can be described approximately as a sum of magnetizations $\mathbf{M}_\mathbf{n}$ homogeneous in each cell $\mathbf{n}$. With a volume of V_s, the latter contains a finite number N_s of localized spins $\mathbf{S}_j$ contributing to the magnetization $\mathbf{M}_\mathbf{n} = -V_s^{-1} \sum_j^{N_s} g\mu_B \langle \mathbf{S}_j \rangle$, where g and μ_B denote the g factor of magnetic ions and the Bohr magneton, respectively. In addition, it can be further assumed that the mean values $\langle \mathbf{S}_j \rangle$ of localized spins in a given cell $\mathbf{n}$ are approximately the same, i.e., $\langle \mathbf{S}_j \rangle \approx -\mathbf{M}_\mathbf{n}/\nu g\mu_B \equiv \langle \mathbf{S}_\mathbf{n} \rangle$, where $\nu = N_s/V_s$. Then, the DMI among the spins belonging to the same cell becomes inactive according to Eq. (9). As such, evaluation of the effective Dzyaloshinskii-Moriya (DM) field $\mathbf{B}_j$ in the above equation simply requires consideration of the contributions from the spin ensemble outside the given cell. This, in turn, allows the following expression for the DM field in terms of magnetizations $\mathbf{M}_\mathbf{n}$ and $\mathbf{M}_{\mathbf{n}'}$:

$$\mathbf{B}_j = -\frac{M_s}{\nu (g\mu_B)^2} \sum_{\mathbf{n}'} \left(\mathbf{m}_{\mathbf{n}'} \times \sum_{j' \in n'} \mathbf{D}_{j,j'} \right), \quad (10)$$

where $\mathbf{m}_\mathbf{n} = \mathbf{M}_\mathbf{n}/M_s$ is the unit vector directed along $\mathbf{M}_\mathbf{n}$. It is implicitly assumed that the magnitude of the magnetization is fixed at the saturation value M_s ($= |\mathbf{M}_\mathbf{n}| = |\mathbf{M}_{\mathbf{n}'}|$) and only its angle or direction varies.

Note that despite the homogeneous magnetization in each cell, the DMI may vary visibly in the length scale d [see Eq. (4)]. When this intracell variation is negligible, the sum over $j' \in n'$ in Eq. (10) can be reduced to the expression $N_s \mathbf{D}(\mathbf{r}_\mathbf{n} - \mathbf{r}_{\mathbf{n}'})$, where $\mathbf{D}(\mathbf{r}_\mathbf{n} - \mathbf{r}_{\mathbf{n}'}) \equiv \mathbf{D}_{\mathbf{n},\mathbf{n}'}$ is taken for any spin pair located at $\mathbf{r}_\mathbf{n}$ and $\mathbf{r}_{\mathbf{n}'}$ in cells $\mathbf{n}$ and $\mathbf{n}'$, respectively. In this picture, the DM field $\mathbf{B}_\mathbf{n}$ in cell $\mathbf{n}$ comes from N_s equally contributing spins, each of which interacts with the surrounding cells $\mathbf{n}'$, i.e.,

$$\mathbf{B}_\mathbf{n} = -\frac{M_s V_s}{(g\mu_B)^2} \sum_{\mathbf{n}'} (\mathbf{m}_{\mathbf{n}'} \times \mathbf{D}_{\mathbf{n},\mathbf{n}'}), \quad (11)$$

where the explicit dependence on the mutual distance of locations $\mathbf{n}$ and $\mathbf{n}'$ [see also Eq. (7)] determines the equation

$$\mathbf{D}_{\mathbf{n},\mathbf{n}'} = \frac{\mathbf{r}_\mathbf{n} - \mathbf{r}_{\mathbf{n}'}}{|\mathbf{r}_\mathbf{n} - \mathbf{r}_{\mathbf{n}'}|} \varphi(\Lambda |\mathbf{r}_\mathbf{n} - \mathbf{r}_{\mathbf{n}'}|) \Delta_{\mathrm{DM}}. \quad (12)$$

In comparison, the explicit dependence of $\mathbf{D}_{j,j'} = \mathbf{D}_{j,j'}(r_{j,j'})$ on the interion distance needs to be accounted for in Eq. (10) if the period of DMI oscillations [Eq. (4)] is comparable to d. When a continuum-type distribution is assumed for the magnetic ions, the effect of the DMI between a pair of spins associated with the $\mathbf{n}'$ and $\mathbf{n}$ cells can be approximated by a mean value $\overline{\mathbf{D}}_{\mathbf{n},\mathbf{n}'}$ over the cell volumes $V_\mathbf{n} = V_{\mathbf{n}'} = V_s$, i.e.,

$$\overline{\mathbf{D}}_{\mathbf{n},\mathbf{n}'} = \frac{1}{V_s^2} \int_{V_n} d\mathbf{r}_\mathbf{n} \int_{V_{n'}} d\mathbf{r}_{\mathbf{n}'} \mathbf{D}_{\mathbf{n},\mathbf{n}'}. \quad (13)$$

This enables a simple substitution of $\mathbf{D}_{\mathbf{n},\mathbf{n}'}$ with the average for the DM field in Eq. (11). In the case of small cell volumes $V_s = d^3$ at $d \ll \Lambda^{-1}$, the result reproduces accurately the interion dependence: $\overline{\mathbf{D}}_{n,n'} = \mathbf{D}_{\mathbf{n},\mathbf{n}'}$ in Eq. (12). Short periods of DMI oscillations or larger dimensions of the cells lead to the deviation of $\overline{\mathbf{D}}_{n,n'}$ from $\mathbf{D}_{\mathbf{n},\mathbf{n}'}$ according to Eq. (13). The approach described above can provide good accuracy while reducing the computational complexity simultaneously.

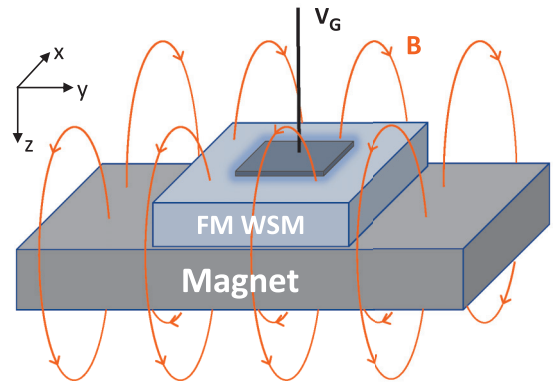

FIG. 1. Schematic illustration of a FM WSM subject to external electric and magnetic fields. The electric field necessary for the chiral anomaly can come from a bias applied to the gate electrode (separated from the WSM by a thin dielectric; not shown), while the stray field $\mathbf{B}$ from a nearby permanent magnet may be used to supply a magnetic field stronger than the intrinsic WSM field.

III. RESULTS AND DISCUSSION

While the long-range asymmetrical spin-spin coupling described above differs qualitatively from the conventional DMI mechanism based on the perturbation of superexchange interaction, its macroscopic effect on magnetic WSMs can lead to spin textures similar to those observed in their nontopological counterparts. A key feature, as stated, is the ability for electrical control. In a bilayer structure with a magnet such as that shown in Fig. 1, the electric field can be provided by a gate, whereas the magnetic field can originate from the stray field of the magnet. Two examples are discussed below.

A. Helical textures

A number of relatively simple DMI effects can be examined without resorting to micromagnetic simulations. A well-known example among them, as discussed earlier, is the magnetization vector canting from the easy axis or easy plane. If the direction of this deviation is not fixed by crystalline anisotropy, the magnetic equilibrium state may form a spiral texture. Thus, it is evident that the present RKKY-type mechanism can be applied to modulate the spiral texture in

WSMs with proper magnetic properties. The analysis requires consideration of the total free energy of the system and its dependence on the characteristic DMI parameter. For simplicity, we consider a magnetic WSM sample subjected to constant electric and magnetic fields applied uniformly along the z axis (i.e., no variation on the x-y plane). Assuming a homogeneous distribution of localized spin moments and a smooth variation of the RKKY-type DMI relative to the atomic scale a ($= \Omega_0^{1/3}$, where Ω_0 denotes the volume of a crystalline primitive unit cell), the density of the WSM magnetic energy associated with the DMI can be approximated by space integrals over a sample volume V_0 instead of sums over the spin moments, i.e.,

$$\begin{aligned}\varepsilon_{\rm DM} &= V_0^{-1}\sum_j\sum_{j'}\mathbf{D}_{j,j'}\cdot\mathbf{m}_j\times\mathbf{m}_{j'}\\ &= \frac{1}{2}n_s c_s\Delta_{\rm DM}\int_{V_0/\Omega_0} d\rho\varphi(\alpha\rho)\frac{\rho}{|\rho|}\cdot\mathbf{m}(a\rho_0)\times\mathbf{m}(a\rho),\end{aligned} \tag{14}$$

where $\rho = \mathbf{r}/a$, $\alpha = \Lambda a$, and n_s and c_s are the number of spins per primitive cell and its density, respectively. This expression also takes into account that $\varepsilon_{\rm DM}$ is invariant to the location $\mathbf{r}_0 = a\rho_0$ of the specific spin used as the reference.

Since finding the total energy minimum is quite complicated in a general case (with additional terms such as the exchange and anisotropy energies), we restrict the consideration to an analysis of the energy change with an intuitive trial function $\mathbf{m}(\mathbf{r})$ mimicking the spiral texture. In the case of axial symmetry around the z axis (which could be easy or hard depending on the sign of the uniaxial anisotropy energy), the simplest trial function depends only on two parameters, i.e., the amplitude β and period L ($= 2\pi/k_c$) of the spatial variation,

$$m(\mathbf{r}) = (\sin\theta\cos\phi, \sin\theta\sin\phi, \cos\theta), \tag{15}$$

where $\sin\theta = \beta$ and $\phi = 2\pi z/L$ ($= k_c z$), while the location $z = 0$ is fixed at the reference magnetization. Substituting Eq. (15) into Eq. (14) yields

$$\varepsilon_{\rm DM} = \beta^2 F_{\rm DM}(\kappa), \tag{16}$$

where the function $F_{\rm DM}(\kappa)$ on $\kappa = k_c a = 2\pi a/L$ is independent of β and is given as

$$\begin{aligned}F_{\rm DM}(\kappa) = \pi n_s c_s\Delta_{\rm DM}\int_0^\infty \rho_\perp d\rho_\perp\int_{-\infty}^{\infty} d\rho_z\frac{\varphi\left(\alpha\sqrt{\rho_\perp^2+\rho_z^2}\right)}{\sqrt{\rho_\perp^2+\rho_z^2}}\\ \times\rho_z\sin\kappa\rho_z.\end{aligned} \tag{17}$$

To reach an energetically favorable configuration, Eq. (17) must take a negative value. This is achieved by choosing an appropriate sign for the parameter κ, which can be positive (clockwise) or negative (counterclockwise configuration) depending on the polarity of $\Delta_{\rm DM}$. In turn, the latter depends on the directions of the applied electric and magnetic fields.

The exchange interaction, anisotropy, and Zeeman energy in an external magnetic field are the main factors tending to keep $\mathbf{m}(\mathbf{r})$ along the easy direction. Their interplay with the DMI establishes the actual parameters β and k_c of the spiral texture. The density of the exchange energy with exchange stiffness A is evaluated by

$$\varepsilon_{\rm ex} = \frac{Aa}{V_0}\iiint_{V_0}\left[\left(\frac{\partial\mathbf{m}}{\partial\rho_x}\right)^2+\left(\frac{\partial\mathbf{m}}{\partial\rho_y}\right)^2+\left(\frac{\partial\mathbf{m}}{\partial\rho_z}\right)^2\right]d\rho_x d\rho_y d\rho_z, \tag{18}$$

which reduces, after a straightforward calculation, to

$$\varepsilon_{\rm ex} = (\beta k_c)^2\frac{Aa}{\Omega_0}. \tag{19}$$

The effect of the uniaxial anisotropy energy $-\frac{1}{2}K_z m_z^2$ depends only on the amplitude of spiral waves,

$$\varepsilon_{\rm an} = -\tfrac{1}{2}K_z(1-\beta^2). \tag{20}$$

As written, the anisotropy constant $K_z > 0$ (<0) corresponds to the case of the easy (hard) z axis. Similarly, the Zeeman energy $-\mathbf{M}\cdot\mathbf{B}$ associated with a relatively weak static magnetic field $|\mathbf{B}| \ll |K_z|/|\mathbf{M}|$ directed along the z axis provides a contribution to the total energy,

$$\varepsilon_{\rm zm} = -M_s B\sqrt{1-\beta^2} \approx -M_s B\left(1-\tfrac{1}{2}\beta^2\right). \tag{21}$$

Interestingly, the total energy minimum in the case of an easy z axis (i.e., $K_z > 0$) occurs at $\beta = 0$ (i.e., $\theta = 0$). Hence, the magnetization in a FM WSM is expected to line up along the z direction uniformly (i.e., no spatial variation and thus no helical waves). Note that our observation does not preclude the formation of any and all textures in the easy-axis WSMs, even those that cannot be described by the ansatz given in Eq. (15). A related example is discussed in Sec. III B.

By comparison, the hard z axis with $K < 0$ leads to an easy x-y plane that is normal to the direction of the magnetic field $\mathbf{B}$. Thus, a chiral magnetic texture may develop on this plane under a DMI, as was shown in an easy-plane antiferromagnet [22]. The stable state of magnetization shows only a small angle deviation δ ($\simeq M_s B/|K_z| \ll 1$) from the plane with $\theta = \frac{\pi}{2} - \delta$ in a relatively weak external magnetic field; thus, $m(\mathbf{r}) \simeq (\cos\phi, \sin\phi, \sin\delta)$. This approximation (i.e., $\beta \approx 1$) simplifies $\varepsilon_{\rm DM}$ and $\varepsilon_{\rm ex}$ to $F_{\rm DM}(\kappa)$ and $\kappa^2\frac{Aa}{\Omega_0}$, respectively, while $\varepsilon_{\rm an}$ and $\varepsilon_{\rm zm}$ are no longer dependent on the parameters of the textures. Subsequently, the minimization of the total energy for $a \ll L$ (thus, $|\kappa| \ll 1$) results in the following simple relation:

$$\kappa = -\frac{F'_{\rm DM}(0)}{2A\Omega_0^{-2/3}}, \tag{22}$$

where $F'_{\rm DM}(0) = \frac{d}{d\kappa}F_{\rm DM}(\kappa)|_{\kappa=0}$. Considering that the azimuthal angle ϕ can be written as $\frac{\kappa}{a}z$, it is evident that the helicity can be realized in the easy-plane FM WSMs even with the DMI of small strength. Figure 2 schematically illustrates the resulting magnetic textures, whose period L is typically in the hundreds of nanometers. For instance, the numerator of Eq. (22) can be estimated from the relation $F'_{\rm DM}(0) = 29\,\pi n_s c_s\Delta_{\rm DM}$ simplified by the choice of $\alpha = 0.8$ (more precisely, $a = 0.8$ nm, $\mathcal{E}_c = 200$ meV, $v_F = 3\times10^7$ cm/s). Then, $\Delta_{\rm DM}$ evaluated with $J = 1$ eV, $\mu_0 = 100$ meV, and $\tau = 5$ ps gives $5\,\mu$eV at $|\mathbf{E}\cdot\mathbf{B}| = 12.5$ kV T/cm and $T_0 = 300$ K. Finally, the use of typical values for n_s ($= 2$), c_s ($= 4\times10^{21}$ cm^{-3}), and A ($= 1.2\times10^{-6}$ erg/cm) yields the characteristic texture period L (or wavelength) of $\approx$320 nm, as stated. Note that this

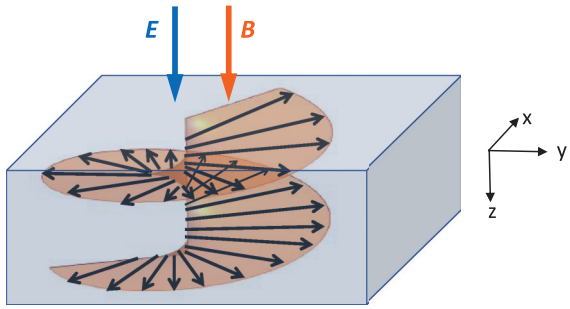

FIG. 2. Magnetic textures generated in the form of a helical wave propagating along the hard z axis.

value for $|\mathbf{E}\cdot\mathbf{B}|$ (i.e., 12.5 kV T/cm) can be achieved with a moderate electric field of tens of kilovolts per centimeter if the (stray) magnetic field can reach a fraction of 1 T or more. For instance, a magnetic field of this magnitude can be readily realized with the neodymium magnet family [23].

B. Magnetic skyrmions

Another well-known phenomenon in which the DMI plays a crucial role is magnetic skyrmions. The analysis of skyrmion stability is far more complex than that for the helical structures described by the analytical expression given in Eq. (15). The problem can be made simpler by the application of micromagnetic simulations described earlier. An easy-axis (z) ferromagnet is considered here since this is a more common condition for skyrmions. To evaluate $\overline{\mathbf{D}}_{\mathbf{n},\mathbf{n}'}$ in Eq. (13), the prefactor $\mathbf{\Phi}_{\mathbf{n},\mathbf{n}'}$ needs to be calculated first as

$$\mathbf{\Phi}_{\mathbf{n},\mathbf{n}'}=\frac{1}{V_s^2}\int_{V_\mathbf{n}}d\mathbf{r}_\mathbf{n}\int_{V_{\mathbf{n}'}}d\mathbf{r}_{\mathbf{n}'}\frac{\mathbf{r}_\mathbf{n}-\mathbf{r}_{\mathbf{n}'}}{|\mathbf{r}_\mathbf{n}-\mathbf{r}_{\mathbf{n}'}|}\varphi(\Lambda|\mathbf{r}_\mathbf{n}-\mathbf{r}_{\mathbf{n}'}|). \quad (23)$$

Assuming cell discretization of d^3 $(=V_s)$ as defined earlier, Eq. (23) takes the form

$$\mathbf{\Phi}_{\mathbf{n},\mathbf{n}'}=\int_{-1/2}^{1/2}d\varrho_x\int_{-1/2}^{1/2}d\varrho_y\int_{-1/2}^{1/2}d\varrho_z\int_{-1/2+l_x}^{1/2+l_x}d\varrho'_x\int_{-1/2+l_y}^{1/2+l_y}d\varrho'_y\int_{-1/2+l_z}^{1/2+l_z}d\varrho'_z\frac{\varrho-\varrho'}{|\varrho-\varrho'|}\varphi(\lambda|\varrho-\varrho'|). \quad (24)$$

Here, $\lambda=\Lambda d$, $\varrho=\mathbf{r}_\mathbf{n}/d$, and $\varrho'=\mathbf{r}_{\mathbf{n}'}/d$, while $\mathbf{l}=(l_x,l_y,l_z)$ with integer values of l_x, l_y, l_z denotes the vector connecting the centers of cells $\mathbf{n}=(0,0,0)$ and $\mathbf{n}'=d(l_x,l_y,l_z)$ in units of cell size d. When λ is sufficiently larger than 1, the RKKY-type interaction (i.e., $\mathbf{\Phi}_{\mathbf{n},\mathbf{n}'}$) decays quickly, and only a small number of neighboring cells needs to be considered in the subsequent sum [e.g., see Eq. (11)]. This point is clearly illustrated in Table I, where the cases of $\lambda=4$ and $\lambda=1.2$ are compared.

To proceed further, let us apply the parameters used in the evaluation of spiral textures. The DM field affecting a particular cell $\mathbf{n}$ consists of the additive contributions of all other cells $\mathbf{n}'$, each of which, in turn, contains N_s spins. Assuming a cell size d of $5a=4$ nm for the micromagnetic simulation, the parameter λ becomes 4 (with the cutoff wave vector $\Lambda=\mathcal{E}_c/\hbar v_F$ set to $1\times10^7\,\mathrm{cm}^{-1}$ earlier in this paper), and N_s $[=n_s\times(d/a)^3]$ amounts to 250 spins (i.e., in each discretized cell). The choice of d appears to be sufficiently small compared to the typical dimension of skyrmions in the tens of nanometers [24]. In addition, the corresponding λ $(=4)$ enables us to truncate the numerical sum to $|\mathbf{l}|\leqslant2$ with good accuracy (see Table I), i.e., 6 nearest-neighbor cells (1,0,0), 12 facial diagonal nearest-neighbor cells (1,1,0), 8 spatial diagonal nearest-neighbor cells (1,1,1), and 6 along the axes with twice the distance of the nearest neighbor (2,0,0). The FM WSM layer is chosen to be sufficiently large (e.g., $200\times200\times16\,\mathrm{nm}^3$) compared to the anticipated size of the skyrmions. In the initial calculation, this layer is assumed to be covered completely by the gate such that the entire WSM is subject to the applied electric field (see Fig. 1). The saturation magnetization $M_s=580\,\mathrm{emu/cm}^3$ and the easy out-of-plane magnetic anisotropy $K_z=2.4\times10^6\,\mathrm{erg/cm}^3$ are also used for the WSM.

As stated, the magnetization dynamics is analyzed by numerically solving the Landau-Lifshitz-Gilbert equation in each cell $\mathbf{n}$ based on Object Oriented MicroMagnetic Framework (OOMMF) [25], i.e.,

$$\frac{\partial\mathbf{m}_\mathbf{n}}{\partial t}=-\gamma\mathbf{m}_\mathbf{n}\times\mathbf{H}_\mathbf{n}^{\mathrm{eff}}+\alpha_g\mathbf{m}_\mathbf{n}\times\frac{\partial\mathbf{m}_\mathbf{n}}{\partial t}, \quad (25)$$

where γ is the gyromagnetic ratio and α_g $(=0.01)$ denotes the Gilbert damping constant. The macroscopic effective field $\mathbf{H}_\mathbf{n}^{\mathrm{eff}}$ can be obtained from the free energy density F of the system as $\mathbf{H}_\mathbf{n}^{\mathrm{eff}}=-(\partial F/\partial\mathbf{m}_\mathbf{n})$, which accounts for the exchange interaction, RKKY-type DMI, anisotropy energy, and Zeeman energy terms:

$$F=\frac{Aa}{2V_0}\sum_{\mathbf{n},\mathbf{n}'\neq\mathbf{n}}\mathbf{m}_\mathbf{n}\cdot\mathbf{m}_{\mathbf{n}'}+\frac{1}{2}\sum_{\mathbf{n},\mathbf{n}'\neq\mathbf{n}}\overline{\mathbf{D}}_{\mathbf{n},\mathbf{n}'}\cdot(\mathbf{m}_\mathbf{n}\times\mathbf{m}_{\mathbf{n}'})-\frac{1}{2}K_z\sum_\mathbf{n}m_{\mathbf{n},z}^2-M_s\sum_\mathbf{n}\mathbf{m}_\mathbf{n}\cdot\mathbf{B}. \quad (26)$$

TABLE I. Numerically evaluated x, y, and z components of the factor $\Phi_{\mathbf{n},\mathbf{n}'}$ [Eq. (24)] reflecting the DMI variation for cells separated by (l_x,l_y,l_z) at different values of λ.

		(l_x,l_y,l_z)								
	Component	(1,0,0)	(1,1,0)	(1,1,1)	(2,0,0)	(2,1,0)	(2,1,1)	(2,2,0)	(2,2,1)	(3,0,0)
$\lambda=4$	Φ_x	0.164	0.0498	0.099	−0.045	−0.039	0.007	0.009	0.004	0.0011
	Φ_y	0	0.0498	0.099	0	−0.019	0.004	0.009	0.004	0
	Φ_z	0	0	0.099	0	0	0.004	0	0.002	0
$\lambda=1.2$	Φ_x	0.193	0.180	0.162	0.289	0.255	0.226	0.176	0.155	0.233
	Φ_y	0	0.180	0.162	0	0.128	0.113	0.176	0.155	0
	Φ_z	0	0	0.162	0	0	0.113	0	0	0

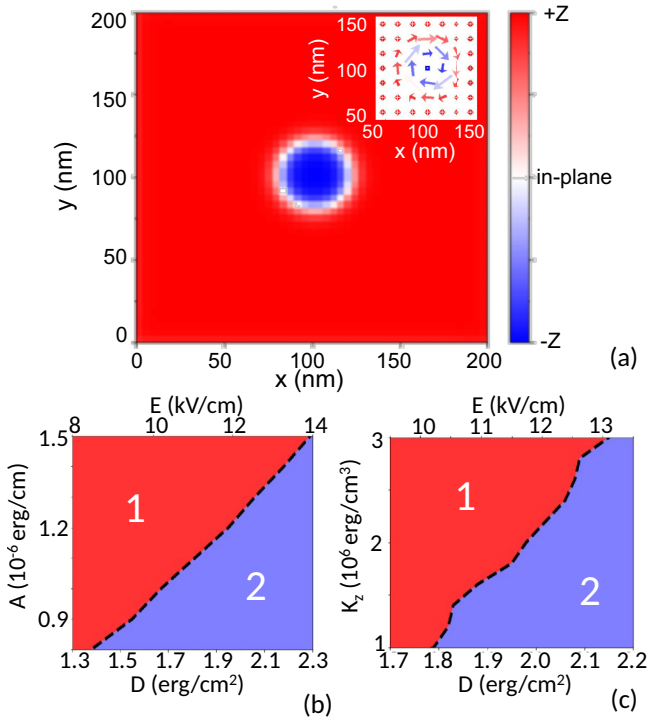

FIG. 3. (a) Snapshot of the simulated magnetic textures in a FM WSM film with $M_s = 580\,\text{emu/cm}^3$, $A = 1.2 \times 10^{-6}\,\text{erg/cm}$, $K_z = 2.4 \times 10^6\,\text{erg/cm}^3$, and $D = 2.06\,\text{erg/cm}^2$. The entire film ($200 \times 200 \times 16\,\text{nm}^3$) is subject to the gate electric field (thus, nonzero DMI). The color code indicates the z component of the magnetization. The inset provides a view of the magnetization directions near the center region. The formation of a stable Bloch skyrmion is observed. (b) and (c) Phase diagrams in the A-D and K_z-D parameter spaces, respectively. The parameter range supported different magnetic textures. In (b), the easy z-axis anisotropy is fixed at $K_z = 2.4 \times 10^6\,\text{erg/cm}^3$, whereas in (c) a constant value is used for the exchange stiffness, $A = 1.2 \times 10^{-6}\,\text{erg/cm}$. Region 1 represents the conditions where the system ground state is the FM phase, while the formation of magnetic textures is energetically favorable in region 2 (i.e., the skyrmion or multidomain phase). The value of the electric field given on the upper horizontal axis is obtained with an assumption of a 1 T magnetic field in the parallel direction.

Here, the summation for the exchange interaction is limited to the nearest neighbors, while the range of nonzero $\overline{\mathbf{D}}_{\mathbf{n},\mathbf{n}'}$ considered is as discussed above (i.e., $|\mathbf{l}| \leqslant 2$). The DMI does not exist outside the gated region since $E = 0$. The Zeeman energy term may be dropped from consideration since its effect is expected to be minor, as discussed in Sec. III A.

The simulation results clearly illustrate that the system can support the formation of stable skyrmions when the conditions are properly adjusted. Figure 3(a) shows a snapshot of magnetic textures, in which a single skyrmion approximately 30 nm in diameter is distinctively visible. Due to the unique property of the RKKY-like DMI, the spins rotate in the tangential planes, resulting in a Bloch-type formation, which is in contrast to the Néel-type textures more commonly found in conventional magnetic thin films. For convenience of the discussion, we introduce a parameter $D = |\overline{\mathbf{D}}_{\mathbf{n},\mathbf{n}'}|d$, with $\mathbf{n} = (0, 0, 0)$ and $\mathbf{n}' = (1, 0, 0)$, as a quantity that effectively signifies the DMI strength. From Eqs. (9), (12), and (13), it is apparent that this parameter D has an explicit dependence on the external fields $\mathbf{E}$ and $\mathbf{B}$. The stable skyrmion formation observed in Fig. 3(a) occurs with the choice of $|\mathbf{E} \cdot \mathbf{B}| = 12.5\,\text{kV T/cm}$, which corresponds to $D \sim 2.06\,\text{erg/cm}^2$.

For a systematic understanding of the conditions necessary for a stable skyrmion state, the dependence on three crucial parameters, i.e., the effective DMI strength D, exchange stiffness A, and magnetic anisotropy K_z, is examined. As discussed, D can be controlled electrically (e.g., via the gate bias; see Fig. 1). In comparison, both A and K_z tend to be more material specific even though the latter may also be modulated externally (e.g., via strain). A parametric analysis is conducted in the A-D and K_z-D spaces, as plotted in Figs. 3(b) and 3(c), respectively. Region 1 represents the conditions where the ground state is the FM phase, while the formation of magnetic textures is energetically stable in region 2. The "boundary" between these two regions can be found as a function of A and K_z, much like that obtained in nontopological ferromagnets with the conventional DMI mechanism [26]. The system in region 2 is driven away from the global FM equilibrium by rotating the magnetization locally toward a lower-energy configuration in either a skyrmion or a multidomain pattern. While the energy minimum actually depends on more than these three parameters, it appears that the values near the boundary tend to give a compact single skyrmion which degenerates into an extended skyrmion or a multidomain state as the conditions move farther away from it. The possibility of individual metastable skyrmions (instead of stable ones) also exists near the critical threshold in region 1. The skyrmion formation shown in Fig. 3(a) corresponds to a location in region 2 close to this demarcation line, as expected. These results strongly indicate that the magnetic textures in the FM WSM can be manipulated actively, for instance, by changing the electric field applied by the gate. One can readily dissolve the skyrmion observed in Fig. 3(a) by simply turning off the gate bias (thus setting $D = 0$). The converse scenario (i.e., creation of skyrmions via electrical control) may also be possible with properly designed excitation conditions overcoming the magnetic anisotropy barrier. The analysis of such dynamical processes is outside the scope of the current study.

Note that the range of modulation in the DMI strength considered here [e.g., from 0 to around $2\,\text{erg/cm}^2$ with a moderate electric field of $\sim$12 kV/cm at $B = 1$ T; see the E-D correspondence in Figs. 3(b) and 3(c)] is far more challenging to attain in conventional ferromagnets. For instance, an electric field as high as 6 MV/cm produced only up to a 10% change in multilayer systems such as Pt/Co/Pd and MgO/Fe/Pt, as detailed in the literature [10,11]. The field needed in the two-dimensional ferromagnet (i.e., CrI_3 monolayer) for a comparable DMI (e.g., $2\,\text{erg/cm}^2$ or $\sim$0.8 meV/atom) was even higher in the 20 MV/cm range [9]. Likewise, the current-induced DMI in the nontopological structures was found to be rather modest, for which maximum modulations of about 0.05 and $0.2\,\text{erg/cm}^2$ were reported in recent studies [13,14] with lateral driving current densities of 4×10^7 and $\sim 7 \times 10^7\,\text{A/cm}^2$, respectively. Evidently, the RKKY-type mechanism enabled by the chiral anomaly can offer a more efficient alternative in magnetic WSMs.

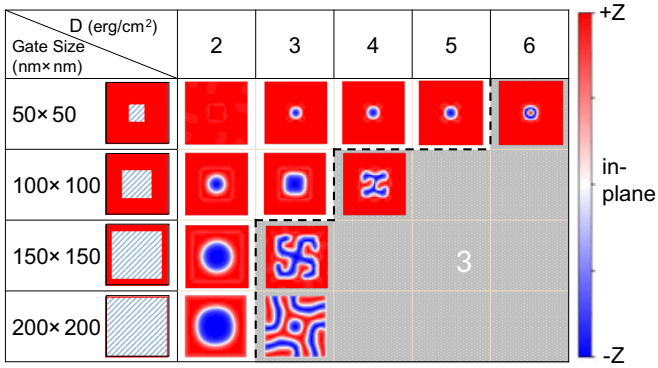

FIG. 4. Phase diagram of gate size vs D in a $200 \times 200 \times 16\,\mathrm{nm}^3$ FM WSM film with $K_z = 1.8 \times 10^6\,\mathrm{erg/cm}^3$; the rest of the parameters are the same as in Fig. 3. In the first column, the gray shaded area indicates the gated region subject to the applied electric field (thus nonzero D). Region 3 denotes the conditions in which a multidomain state is the energy minimum. Snapshots are taken once the magnetization reaches a stable state.

The issue of a single skyrmion vs a multidomain and its dependence on D (i.e., the effective DMI strength) is further investigated along with the impact of finite sizes in the gate electrode (i.e., the region in which the electric field is applied). The interaction between the nonzero and zero DMI regions of the WSM (i.e., inside and outside the gated area) introduces a boundary condition that can affect the stability of the textures, particularly when the two dimensions are comparable to each other. Figure 4 shows snapshots of the spin textures obtained for different gate sizes and DMI strengths. Note that a K_z of $1.8 \times 10^6\,\mathrm{erg/cm}^3$ is used in this calculation [vs $2.4 \times 10^6\,\mathrm{erg/cm}^3$ in Figs. 3(a) and 3(b)], while the rest of the material properties remain unchanged. The choice of a smaller K_z leads to generally larger magnetic textures, enabling us to better illustrate the significance of these two parameters under consideration.

Our simulation results confirm that for a given gate size, a stronger DMI (i.e., D) leads to larger skyrmions and, eventually, to a multidomain state (denoted as region 3, a subset of region 2 in Fig. 3), which is consistent with the phase diagram shown earlier. This trend continues as the gated region shrinks, albeit with the transition occurring at a progressively larger D. Incidentally, a smaller gate also results in a more compact skyrmion despite the identical material properties. In fact, stable single skyrmions can be observed even when the size of the gate is smaller than that of a "free" skyrmion unconstrained by the gate boundary (e.g., see the cases with 50×50 and $100 \times 100\,\mathrm{nm}^2$ vs that with $200 \times 200\,\mathrm{nm}^2$). Apparently, the true impact of D is determined not only by its strength but also by its spatial extent. As such, a smaller gate would require a stronger D for the onset of skyrmion formation and keep it compact over an extended range before its degeneration into multidomain textures. Compared to its counterparts in nontopological materials [24], this influence of the gate size clearly reveals another means to control skyrmions in magnetic WSMs along with the common dependence on such parameters as the DMI strength, magnetic stiffness, and magnetic anisotropy (see also Fig. 3). The chiral anomaly enabled long-range DMI mechanism provides a unique opportunity for electrical control of spin textures in magnetic WSMs.

IV. SUMMARY

Among their numerous fascinating traits, WSMs possess an unusual DM-like remote spin-spin interaction mediated by Weyl fermions. As the symmetry dictates, this interaction disappears in a crystal with centrosymmetry. However, the invariance to inversion can be lifted in the presence of external electric and magnetic fields. While these fields have only a minor effect on the crystalline structure itself, the node polarization stemming from the chiral anomaly can break the symmetry and dramatically enhance this RKKY-type DMI in magnetic WSMs. Our quantitative analysis clearly showed that even a moderate strength of the external fields can induce a DMI sufficiently strong to curl the local magnetic moments into incommensurate magnetic textures such as helical waves and skyrmions. The explicit dependence of this DMI mechanism on external fields clearly illustrates the possibility of active modulation in the resulting magnetic textures for efficient WSM-based spintronic applications. The influence of other key parameters, such as magnetic stiffness and magnetic anisotropy, on stable texture formation was examined comprehensively as well.

ACKNOWLEDGMENT

This work was supported, in part, by the U.S. Army Research Office (Grant No. W911NF-20-2-0166).

[1] I. Dzyaloshinsky, A thermodynamic theory of weak ferromagnetism of antiferromagnetics, J. Phys. Chem. Solids **4**, 241 (1958).

[2] T. Moriya, Anisotropic superexchange interaction and weak ferromagnetism, Phys. Rev. **120**, 91 (1960).

[3] A. F. Andreev and V. I. Marchenko, Symmetry and the macroscopic dynamics of magnetic materials, Sov. Phys. Usp. **23**, 21 (1980).

[4] P. Tolédano, A. P. Ayala, A. F. G. Furtado, J. P. C. do Nascimento, M. A. S. Silva, and A. S. B. Sombra, Magnetoelectric effects in the spiral magnets $CuCl_2$ and $CuBr_2$, J. Phys.: Condens. Matter **29**, 035701 (2017).

[5] B. A. Ivanov and D. D. Sheka, Soliton (vortex) thermodynamics of a quasi-2D easy-plane antiferromagnet, JETP **80**, 907 (1995).

[6] A. N. Bogdanov and C. Panagopoulos, Physical foundations and basic properties of magnetic skyrmions, Nat. Rev. Phys. **2**, 492 (2020).

[7] Y. Zhang, J. Liu, Y. Dong, S. Wu, J. Zhang, J. Wang, J. Lu, A. Rückriegel, H. Wang, R. Duine, H. Yu, Z. Luo, K. Shen, and

J. Zhang, Strain-driven Dzyaloshinskii-Moriya interaction for room-temperature magnetic skyrmions, Phys. Rev. Lett. **127**, 117204 (2021).

[8] D. A. Kitchaev, I. J. Beyerlein, and A. Van der Ven, Phenomenology of chiral Dzyaloshinskii-Moriya interactions in strained materials, Phys. Rev. B **98**, 214414 (2018).

[9] J. Liu, M. Shi, J. Lu, and M. P. Anantram, Analysis of electrical-field-dependent Dzyaloshinskii-Moriya interaction and magnetocrystalline anisotropy in a two-dimensional ferromagnetic monolayer, Phys. Rev. B **97**, 054416 (2018).

[10] T. Koyama, Y. Nakatani, J. Ieda, and D. Chiba, Electric field control of magnetic domain wall motion via modulation of the Dzyaloshinskii-Moriya interaction, Sci. Adv. **4**, eaav0265 (2018).

[11] W. Zhang, H. Zhong, R. Zang, Y. Zhang, S. Yu, G. Han, G. L. Liu, S. S. Yan, S. Kang, and L. M. Mei, Electrical field enhanced interfacial Dzyaloshinskii-Moriya interaction in MgO/Fe/Pt system, Appl. Phys. Lett. **113**, 122406 (2018).

[12] J. Lu, L. Si, Q. Zhang, C. Tian, X. Liu, C. Song, S. Dong, J. Wang, S. Cheng, L. Qu, K. Zhang, Y. Shi, H. Huang, T. Zhu, W. Mi, Z. Zhong, L. Gu, K. Held, L. Wang, and J. Zhang, Defect-engineered Dzyaloshinskii-Moriya interaction and electric-field-switchable topological spin texture in $SrRuO_3$, Adv. Mater. **33**, 2102525 (2021).

[13] G. V. Karnad, F. Freimuth, E. Martinez, R. Lo Conte, G. Gubbiotti, T. Schulz, S. Senz, B. Ocker, Y. Mokrousov, and M. Kläui, Modification of Dzyaloshinskii-Moriya-interaction-stabilized domain wall chirality by driving currents, Phys. Rev. Lett. **121**, 147203 (2018).

[14] N. Kato, M. Kawaguchi, Y.-C. Lau, T. Kikuchi, Y. Nakatani, and M. Hayashi, Current-induced modulation of the interfacial Dzyaloshinskii-Moriya interaction, Phys. Rev. Lett. **122**, 257205 (2019).

[15] H.-R. Chang, J. Zhou, S.-X. Wang, W.-Y. Shan, and D. Xiao, RKKY interaction of magnetic impurities in Dirac and Weyl semimetals, Phys. Rev. B **92**, 241103(R) (2015).

[16] M. V. Hosseini and M. Askari, Ruderman-Kittel-Kasuya-Yosida interaction in Weyl semimetals, Phys. Rev. B **92**, 224435 (2015).

[17] S.-X. Wang, H.-R. Chang, and J. Zhou, RKKY interaction in three-dimensional electron gases with linear spin-orbit coupling, Phys. Rev. B **96**, 115204 (2017).

[18] P. Nikolić, Dynamics of local magnetic moments induced by itinerant Weyl electrons, Phys. Rev. B **103**, 155151 (2021).

[19] M. Sherafati and S. Satpathy, RKKY interaction in graphene from the lattice Green's function, Phys. Rev. B **83**, 165425 (2011).

[20] K. Fukushima, D. E. Kharzeev, and H. J. Warringa, Chiral magnetic effect, Phys. Rev. D **78**, 074033 (2008).

[21] J. D. Hannukainen, A. Cortijo, J. H. Bardarson, and Y. Ferreiros, Electric manipulation of domain walls in magnetic Weyl semimetals via the axial anomaly, SciPost Phys. **10**, 102 (2021).

[22] Y. G. Semenov, X.-L. Li, X. Xu, and K. W. Kim, Helical waves in easy-plane antiferromagnets, Phys. Rev. B **96**, 224432 (2017).

[23] J. Fraden, *Handbook of Modern Sensors: Physics, Designs, and Applications*, 4th ed. (Springer, New York, 2010), p. 73.

[24] X. Xu, X.-L. Li, Y. G. Semenov, and K. W. Kim, Creation and destruction of skyrmions via electrical modulation of local magnetic anisotropy in magnetic thin films, Phys. Rev. Appl. **11**, 024051 (2019).

[25] M. J. Donahue and D. G. Porter, *OOMMF User's Guide*, version 1.0 (NIST, Gaithersburg, MD, 1999).

[26] S. Rohart and A. Thiaville, Skyrmion confinement in ultrathin film nanostructures in the presence of Dzyaloshinskii-Moriya interaction, Phys. Rev. B **88**, 184422 (2013).